UNIVERSITY OF TARTU

Faculty of Science and Technology

Institute of Technology

Madis Ollikainen

COMPUTER SIMULATIONS OF SINGLE-ION BAB TRIBLOCK COPOLYMER ELECTROLYTE MATERIAL FOR LITHIUM-POLYMER BATTERIES

Bachelor's thesis (12 ECTS)

Supervisor:
Heiki Kasemägi

Tartu   2014

Contents

Introduction

Driven by potentially immense impact on the environment and energy security, electrification of the transport sector has been rapidly accelerating in the 21th century [1]. A major issue for hybrid and full electric cars is power supply. Battery performance greatly depends on their basic building blocks: two active electrodes and an ion-conductive electrolyte connecting them [2]. The electrodes differ in chemical potential enabling electricity generation when they are externally connected, while the charge balance is kept by ion transfer through the electrolyte, which also acts as a separator to avoid internal short-circuiting. Secondary batteries can be recharged with applying a reverse voltage greater than the original forward voltage.

Currently dominant Li-ion batteries [3] employ Li^+ transfer between the electrodes, typically graphite and a Li transition metal complex, most often $LiCoO_2$ [2, 4]. Their theoretical maximum energy density is estimated to be 300–400 $Wh\,kg^{-1}$, which would not be enough to give electric vehicles the distance range of gasoline driven cars [3]. Achieving the necessary energy and power density requires development of novel materials for both the active electrodes and electrolyte [2, 5]. Lithium metal anode combined with air or sulfur cathodes seems one of the most promising solution for the future [3, 6]. Although liquid electrolytes have higher ionic conductivity compared to dry systems, they introduce numerous safety hazards, especially when in contact with Li metal [7]. Consequently, solid-state electrolytes would be preferable [8].

Alas, due to irregular metallic lithium deposition during recharge, usage of lithium metal anode introduces an increased risk of dendrite formation, which can short-circuit the electrodes [9, 10]. A proposed solution would be to employ an electrolyte material with high elastic modulus [7, 11]. For real-world applications the cost, availability and environmental impact of the components must also be taken into account [2]. Thus organic polymer electrolytes are favorable to metal-oxide electrolytes, even though the later tend to have higher elastic modulus [7, 12]. Recently, considerable effort has been deployed into researching renewable solid polymer electrolytes (SPE) [13], which would reduce the carbon-footprint of the battery industry [2].

Understanding the fundamental processes governing SPE properties could substantially improve the development of more efficient materials [14]. While experimental methods provide enormous amounts of information, there are aspects, which are complicated to be analyzed with measured data alone and would greatly benefit from comprehensive theoretical treatment [14, 15]. Modern computational resources have enabled employing theoretical studies using numerical simulations. Investigating the molecular level structure and dynamics, for example, merits greatly form these [16, 17]. Computational approaches also provide tools for determining optimal nano- and microscopic geometrical compositions and predict potentially superior materials' formulations [18].

Even with contemporary powerful computers it is not feasible nor practical to simulate all systems in the most fundamental theoretical framework [17]. Quantum mechanical treatment tends to be computationally very expensive and often can't be applied because the representative unit of the system of interest is far to big to be tackled. Nevertheless, many fully atomistic phenomena can be simulated using the classical molecular dynamics methodology, which treats atoms as point masses, whose interactions are described using classical potentials, and solves for the time evolution in the framework of Newtonian mechanics [19].

The present work focuses on a family of single-ion BAB triblock copolymer electrolytes recently proposed by Bouchet *et al* [20], which are composed of poly(styrene trifluoromethanesulphonylimide of lithium) P(STFSILi) based polyelectrolyte B-blocks and a linear poly(ethylene oxide) PEO A-block. The material exhibited a promising combination of conductive and mechanical properties, as well as an intriguing response to temperature change and P(STFSILi) chain length variation. Probing this behavior on the atomistic scale via classical molecular dynamics (MD) simulations is the main aim of the present work. Additionally, several dihedral angle potentials, necessary for the MD force field compilation, are calculated from density functional theory (DFT).

The thesis is structured into four parts. Chapter 1 introduces the basics of SPEs and PEO based system specifically, presents a short selection of computational studies and gives an overview of the BAB triblock copolymer material considered in this work. Theoretical concepts underlaying MD and DFT are provided in chapter 2. The simulation setups and workflow are described in chapter 3 and discussion of the results in chapter 4.

Chapter 1

Background

1.1 Solid polymer electrolytes (SPEs)

Works by Wright and co-workers [21, 22] in 1973-75, reporting ionic conductivity in poly(ethylene oxide) complexes with sodium salts, have been marked as the beginning of solid polymer electrolyte (SPE) development [8]. Their usage in lithium based systems was proposed by Armand [23] already in 1978. To this day one of the primary issues in deploying fully SPE based batteries on an industrial scale has been too low ionic conductivity [14]. According to Meyer [24] values higher than $10^{-5}\,\mathrm{S\,cm^{-1}}$ in the temperature range of $-20\,°\mathrm{C}$ to $+60\,°\mathrm{C}$ have to be achieved, while others [25, 26] find that at least $10^{-4}\,\mathrm{S\,cm^{-1}}$ at room temperature is necessary.

Salts and polymers can interact by solvation of cations, anion, or both in the polymer matrix [27] – SPEs are essentially dry solutions of alkali metal salts in a polymer host matrix. Usually the conduction ion is a cation e.g. $\mathrm{Li^+}$, as their dissolving is enabled by periodical sites of unshared electron pairs, such as $-\mathrm{O}-$, $-\mathrm{S}-$, $-\mathrm{N}-$, $-\mathrm{P}-$, $\mathrm{C=O}$ and $\mathrm{C=N}$ [27]. Since ionic conductivity is approximately proportional to number, charge and mobility of free ions in the electrolyte, one is interested in maximising the degree of dissociation of Li salts [24]. This can be achieved with salts that have low lattice energy and host polymers with high dielectric constant [24]. Highest fraction of dissociated ions have been reported at concentrations around [O]:[Li] = 25 [24].

The salt solvation is mostly dependant on the interaction between the cation and the polymer host [28]. Best suited are small cations without easily polarizable valence electrons like $\mathrm{Li^+}$, $\mathrm{Na^+}$, $\mathrm{Mg^{2+}}$. On the other hand anions, which usually are not solvable in polymers, should preferably be large and have a delocalized charge. This increases the anion stability

in the electrolyte as well as decreases the lattice energy of the salt, improving the degree of dissociation. Amongst the most practical and widely studied anions are ClO_4^-, BPh_4^-, PF_6^-, BF_4^-, $CF_3SO_3^-$ and $(CF_3SO_2)_2N^-$. [28]

Dissociation of salts generates both cations and anions, leading to dual ion conduction [29]. Nevertheless, only cations are changed with the electrodes. Anion conduction generates a ion concentration gradient. This is believed to contribute greatly to the risk of lithium metal dendrites growth, which could lead to short circuiting the electrodes [30]. Therefore, obtaining a material with Li^+ transport number – the fraction of charge carried by Li^+ compared to the whole charge transfer – as close to one as possible is desired [25, 26]. One of the possible solutions would be to employ polymers, with ionizable groups – polyelectrolytes [31] –, that would allow for single-ion conduction via having the anion covalently bonded to the polymer matrix [24]. For example, P(STFSILi) has been successfully applied to increase the Li^+ transport number [20, 29].

A major obstacle for implementing SPEs is finding a polymer with both high ionic conductivity and great mechanical properties [7].A great deal of research has been dedicated towards constructing materials with higher ionic conductivity at room temperature [28]. For example superior conductivities, i.e. 10^{-2}–$10^{-4}\,S\,cm^{-1}$, have been achieved via addition of plasticizers to the degree of generating a solid-liquid intermediate gel electrolyte [28, 32]. Unfortunately this and many other novel solutions for enhancing conductivity tend to decrease the mechanical properties and stability of the electrolyte, especially in contact with lithium metal electrodes [26, 28]. It is necessary consider the motivations for introducing dry solid polymer electrolytes in the first place: mechanical, thermal and electrochemical stability, compatibility with Li metal electrode and availability of raw materials [25, 26, 28].

1.2   Poly(ethylene oxide) (PEO)

The historically first polymer host poly(ethylene oxide) (PEO; $-[CH_2CH_2O]_n-$) has become the most frequent base for the development of new materials [28]. PEO can exist both in a amorphous and crystalline phase. The helical crystal structure of PEO might be speculated to work as a conduction pathway. This was disproven by Berthier *et al.* [33] in 1983. Employing nuclear magnetic resonance techniques, they showed that the crystalline phase of PEO does not partake in the ion conduction. Although, in 2001 Gadjourova *et al.* [34] yet again overturned this view, by demonstrating higher conductivity for crystalline complexes $LiXF_6 \cdot PEO_6$ (X = P, As or Sb) than their amorphous counterparts. Nevertheless, the measured conductivities were still much lower than achieved with amorphous polymers.

It is now a widely held belief, that the fast ion conduction is promoted by the segmental motion of the amorphous phase [24, 28]. Implementations of classical molecular dynamics simulations [35] and *ab initio* quantum mechanical calculations [36] have suggested, that Li^+ is on average complexed by four to six PEO oxygen atoms. The polymer motion induced breaking of Li^+ and PEO co-ordination bonds and formation of new ones is thought to be behind the ion migration. In principle, Li^+ jumps from one complexation site to another, either along the polymer chain or between neighboring chain segments. However, this is only a model description, the exact mechanism of ion transport is not yet known [28].

In order to achieve higher conductivities at ambient temperatures, research has been aimed at materials with low glass transition temperatures T_g [24]. Poly(propylene oxide) (PPO; $-[CH(CH_3)CH_2O]_n-$) might be viewed as valid option for this. The methyl groups, which are arranged randomly, prevent the polymer from forming a crystalline structure [28]. Alas these methyl groups also impede the segmental motion of the polymer as well as the cation solvation. Consequently, PEO is more commonly used.

A successful method for suppressing the crystallization in PEO has been the introduction of random copolymers [28]. Specifically random insertion of either methylene oxide $(-CH_2O-)$ or dimethyl siloxy $(-Si(CH_3)_2O-)$ groups into the PEO chain prevents the helical crystal structure formation. Also crafting low molecular weight polyether side chains to the polymer backbone can enhance the conductivity or mechanical strength, although usually when one is improved the other is degraded. Alternatively, using block copolymer structures allows to combine polymers with good conductivity to those with great mechanical strength. [28]

1.3   Computer simulations of polymer electrolytes

Modern high performance computational capabilities provide an extremely useful tool for investigating the atomistic level phenomena in polymer electrolytes. For example molecular dynamics simulations have given insight into the specific conduction mechanisms of Li^+ in both amorphous [35] and crystalline [37] PEO. For both the Li^+ is essentially jumping between different complexation sites. While in the amorphous phase, the driving mechanism is related to the chain motion, in crystalline phase, structural perturbations and interactions with the anion seem to be the case.

Quantum mechanical methods can be implemented to more accurately probe PEO–Li^+ interaction. Based on small model systems [36], Li^+ has been reported to coordinate to 4–6 oxygens, with a average distance around $2\,Å$. An other application of quantum mechanical

calculations is to develop a set of interaction potentials, also called the *force field*, for use in classical molecular dynamics simulations [38–41]. For example, the force field generated for PEO by Neyertz *et al.* [41] replicated the X-ray diffraction data for PEO crystalline structure and has been extensively used afterwards [37, 42–44].

Recently the P(STFSI)/PEO [29] blend, a polymer system very similar to the one simulated in the present work, has been modeled by Brandell *et al* [44]. These simulations indicated that the composed force field produced realistic diffusion coefficients in the order of $10^{-13}\,\mathrm{m^2\,s^{-1}}$, which are comparable to experimental results [45]. However, the coordination of Li^+ to PEO oxygen was found to be $6-7$, which is higher than the expected values of $4-6$ [35, 36]. Whether this is a feature of the force field or the specific material remains unknown.

1.4   P(STFSILi)-PEO-P(STFSILi)

Bouchet *et al.* [20] have recently reported synthesizing a family of single-ion BAB copolymer electrolytes with empirical formula $P(STFSILi)_p-PEO_n-P(STFSILi)_p$, Fig. 1.1 illustrates the corresponding repetitive units. Their conductive properties indicate some interesting trends with temperature and P(STFSILi) chain length variation. The present work aims at further studying of these relations via implementations of computer simulations. Table 1.1 describes the different chain lengths considered by Bouchet *et al.* [20] and the corresponding systems investigated in the present work.

At temperatures above $55\,^{\circ}\mathrm{C}$ polymers BAB11 and BAB15 (see table 1.1) demonstrated the highest experimentally found conductive properties followed by BAB24, BAB06 and BAB41. Steady exponential decrease of conductivity with temperature was reported for all chain lengths, until the three shorter developed a steep drop of 1–2 of order of magnitude at $60\,^{\circ}\mathrm{C}$ for BAB06 and $55\,^{\circ}\mathrm{C}$ for BAB11 and BAB15. The larger polymers, on the other hand continued their steady descend. Figure 2 of the experimental paper [20] better illustrates this behavior.

Some rather promising properties is produced by the poly(styrene trifluoromethanesulphonylimide of lithium) based B-block acting both as a Li^+ salt and a plasticizer. First, the combination of the delocalized charge of the $TFSI^-$ anion and the polyelectrolyte nature of the B-block rises Li^+ transport number above 0.85. Single-ion conductivity of $1.3 \cdot 10^{-5}\,\mathrm{S\,cm^{-1}}$ reported at $60\,^{\circ}\mathrm{C}$ is also quite satisfactory. Additionally, the polymer has a electrochemical stability window up to 5 V compared to Li/Li^+. The reported stress-strain tests at $40\,^{\circ}\mathrm{C}$ show approximately an order of magnitude higher Young's modulus than a similar system of $PS-PEO-PS$ doped with TFSILi. It is proposed that this could be

due to strong ionic crosslinking between the PEO and P(STFSILi), which might increase the durability of future battery systems. [20]

Experimental				
Name	M(PEO) g mol^{-1}	M(P(STFSILi)) g mol^{-1}	Wt% of P(STFSILi)	[EO]:[Li]
BAB06		2×1850	9.5	69
BAB11		2×3600	17	36
BAB15	35000	2×4750	21.4	27
BAB24		2×7800	31	16
BAB41		2×13200	43	10
Simulations				
Name	n	p	Wt% of P(STFSILi)	[EO]:[Li]
BAB06		$5.76 \approx 6$	9.9	66.3
BAB11		$11.2 \approx 11$	16.8	36.2
BAB15	$795.5 \approx 796$	$14.8 \approx 15$	21.5	26.5
BAB24		$24.3 \approx 24$	30.5	16.6
BAB41		$41.12 \approx 41$	42.9	9.7

Table 1.1: Descripton of the different chain lengths for P(STFSILi)$_p$−PEO$_n$−P(STFSILi)$_p$ in both experimental work done by Bouchet *et al.* [20] and for simulations done in this work. Wt% denotes mass fraction, n and p the lengths of the corresponding chain segments and [EO]:[Li] the PEO oxygen to Li ratio in the polymer.

(a) P(STFSILi)

(b) PEO
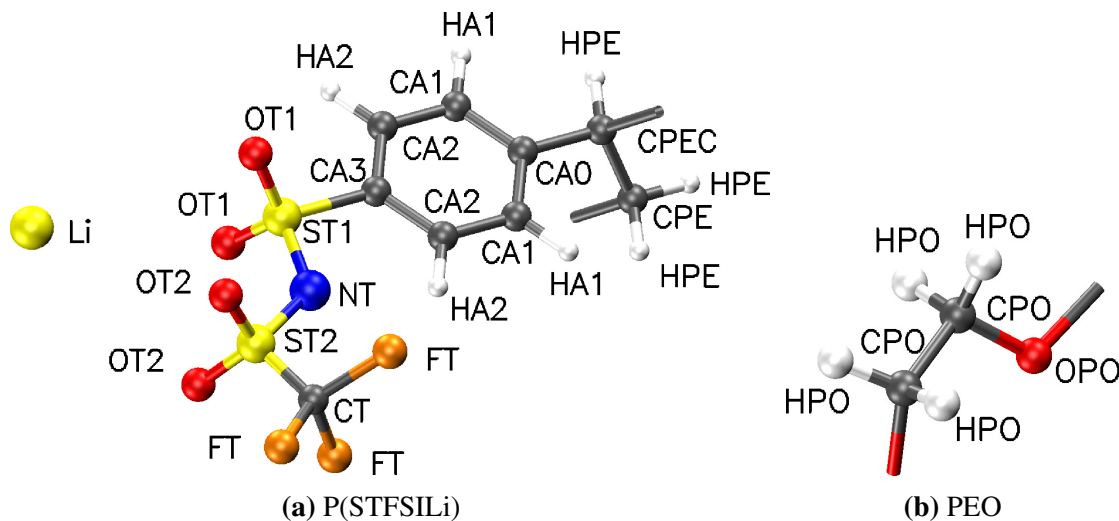
Figure 1.1: Corresponding repetitive units with atom labels used in the present thesis

Chapter 2

Computer simulations: theoretical background

The vibrational kinetic energy of nuclei is roughly two orders of magnitude smaller, but their mass much greater, than those of the electrons. Consequently it is justified to use the Born-Oppenheimer approximation of separating the Schrödinger equation into electronic and nuclear parts, such that the electronic wave function depends only on the position of the nuclei, but not their velocities, and its solution determines the potential energy for the nuclear Schrödinger equation. Furthermore, in most cases the nuclei are heavy enough to be reasonably modeled as classical particles moving on the potential energy surface (PES), defined by the solution to the electronic Schrödinger equation. This is the underlying foundation of atomistic simulations. [46]

Many techniques have been formulated for describing the PES. Choosing the best fitted method depends on the nature of the problem at hand, necessary accuracy and available computational resources. Arguably the most obvious way to find the PES would be solving the electronic Schrödinger equation. For this end, a variety of approaches have been developed, such as Hartree-Fock, many-body perturbation and density functional theory to name a few. These tend to be computationally very demanding and often only simulations with up to several hundred atoms are feasible. For larger systems, phenomena that are not dominated by quantum effects can be investigated with so-called *force field* methods: molecular mechanics (MM) and molecular dynamics (MD). [46]

The polymer electrolyte systems, considered in the present work, consist of several thousand atoms. Therefore being too big to tackle with quantum mechanical methods, rather the MD technique was chosen, as it has previously [37, 42–44] been successfully employed for studying

Li$^+$ conduction mechanisms. Most of the force field for describing the PES could be combined from published works [39, 41, 44, 47–51], while the missing components where calculated using density functional theory (DFT). In the following chapter an overview of the physical concepts, underlying MD and DFT, are presented. The theory presented in this chapter is primarily based of textbooks [19, 46] for quantum mechanical methods and [19, 52, 53] for force field methods. Unless any other specific reference is given, these should be considered as referenced throughout the corresponding parts of the following chapter.

2.1 Quantum mechanical methods

2.1.1 Molecular orbitals and basis sets

In order to make the calculations more feasible the electronic wave function Ψ is approximated as a superposition of one-electron wave functions ψ – so called orbitals. For single atoms and molecular systems these are called atomic and molecular orbitals, respectively. In non-relativistic framework the electron spin must be introduced *ad hoc*. This divides each molecular orbital into two spin-orbitals $\chi_{1,2}$. The antisymmetry of Ψ is ensured by calculating it as an Slater determinant

$$\Psi = \frac{1}{\sqrt{N}} \begin{vmatrix} \chi_1(1) & \chi_2(1) & \cdots & \chi_N(1) \\ \chi_1(2) & \chi_2(2) & \cdots & \chi_N(2) \\ \vdots & \vdots & \ddots & \vdots \\ \chi_1(N) & \chi_2(N) & \cdots & \chi_N(N) \end{vmatrix}, \tag{2.1}$$

where N is the number of electrons in the system. The first row corresponds to assigning the "first" electron to all of the spin-orbitals, the second to assigning the "second" electron to all of the spin-orbitals etc.

As the form of the molecular orbitals are unknown, they are further approximated by a linear combination of finite number of known functions called the basis set. Obviously the choice of the basis set plays a significant role in calculations quality. The primary considerations when picking a basis set are: (a) their shape should be able to describe the physics involved; (b) they should minimize the computational effort. Plain waves based sets are rather customary when dealing with periodic systems, like crystals. For isolated molecules common implementations are inspired by the analytical solutions to the hydrogen atom – thus they are often called atomic orbitals. Considering the hydrogen atom, it would be ideal to use functions with an analytical

form of

$$\chi_{\zeta,n,l,m}(r, \Theta, \phi) = N Y_{l,m}(\Theta, \phi) r^{n-1} e^{-\zeta r}, \qquad (2.2)$$

where N is the normalization constant and $Y_{l,m}(\Theta, \phi)$ is the spherical harmonic. These are called Slater type basis functions. Due to computational considerations they are often approximated with Gaussian type functions

$$\chi_{\zeta,n,l,m}(r, \Theta, \phi) = N Y_{l,m}(\Theta, \phi) r^{2n-2-l} e^{-\zeta r^2}. \qquad (2.3)$$

While increasing the size of the basis set improves the quality of the calculations, it considerably rises the computational resources needed as well. Choosing an optimal number of basis functions is of substantial relevance. Minimal basis set for describing an atom has as many functions as there are electrons in the atom. A significant improvement is gained by doubling the minimum basis. Such sets are named *double-dzeeta* or DZ basis sets, after the commonly used ζ in the exponent in (2.2) and (2.3). Triple-dzeeta basis sets are also frequently used. As most phenomena of interest are essentially dictated by the valence electrons, so-called split valence basis sets are used. In these only the valence electrons are described by double (DZ) or triple number (TZ) of minimal basis sets. Furthermore, basis functions describing the core electrons are often contracted, i.e. full basis set is combined into a smaller one by fixed linear combinations. This results in remarkable rise in computational efficiency via a small loss of accuracy.

The quality of the basis set can be enhanced by introducing polarization and/or diffuse functions to generate more "realistically shaped orbitals". Polarization is achieved by functions with higher orbital quantum number. For example s-orbitals can be polarized with addition of functions describing p-orbitals, while p-orbitals can be polarized with functions describing d-orbitals. As Gaussian basis functions degrade very fast with the growth of the radial coordinate, diffuse functions – functions with low maximum and gentle decline – help better represent loose electrons, that are far from the nuclei. Addition of polarization and diffuse functions are denoted with "$*$" or "(d, p)" and "$+$" or "*aug*" respectively.

2.1.2 Density functional theory (DFT)

DFT is based on the two Hohenberg-Kohn theorems [54]. The first of which shows that the ground state properties of electronic systems can be derived from the electron density and the second defines the energy functional of the system and proves that the ground state electron density minimizes it. Effectively reducing a problem with $3N$ spatial coordinates to a 3 spatial

coordinates problem. Assuming the exact form of the energy functional is known – which it is not. Nevertheless employing a set of approximations DFT has become one of the most popular computational methods in solid state physics and quantum chemistry [55].

In Born-Oppenheimer approximation, where interaction between the nuclei can be ignored, the energy functional can be divided into three parts: (a) kinetic energy $T[\rho]$, (b) attraction between nuclei and electrons $E_{ne}[\rho]$ and (c) electron-electron repulsion $E_{ee}[\rho]$. The last can yet again be separated into Coulomb $J[\rho]$ and exchange $K[\rho]$ parts

$$E_{DFT}[\rho] = T[\rho] + E_{ne}[\rho] + J[\rho] + K[\rho]. \tag{2.4}$$

$J[\rho]$ and $E_{ne}[\rho]$ can be expressed analogously to their classical counterparts, but the analytical form of $E_{ee}[\rho]$ and $K[\rho]$ are unknown. This was overcome by Kohn and Sham [56] with the reintroduction of basis functions, which allowed expressing the kinetic energy

$$T[\rho] = T_S[\rho] + T_\Delta[\rho], \tag{2.5}$$

where the bulk part of the kinetic energy $T_S[\rho]$ can be calculated analytical from the exact Slater determinant and $T_\Delta[\rho]$ is a small correction functional. Thus the whole energy can be expressed as

$$E_{DFT}[\rho] = T_S[\rho] + E_{ne}[\rho] + J[\rho] + \underbrace{K[\rho] + T_\Delta[\rho]}_{E_{XC}[\rho]}. \tag{2.6}$$

Several estimations have been proposed for the exchange-correlation term $E_{XC}[\rho]$. These can roughly be divided into three groups: local density approximation (LDA), generalized gradient approximation (GGA) and hybrid functionals. In the framework of LDA the electron density is considered to have a slow spatial change, so that it can be estimated to be locally constant, while the GGA approach characterizes it with both a local value and a gradient. Hybrid functionals on the other hand consist of linear combinations of the exact exchange energy in the Hartree-Fock framework[1] and energies found from different LDA and GGA functionals.

The reintroduction of basis functions means that the practical DFT methods applied nowadays are not anymore dependent only of three spatial coordinates, but also of the basis set. Thus accuracy of the calculations are determined by both the choice of basis set and the approximation for the exchange-correlation term $E_{XC}[\rho]$. Nevertheless DFT methods tend to provide rather reasonable results with comparatively cheap computational costs, making them

---

[1]This arises a legitimate question: why not calculate the whole exchange energy from Hartree-Fock theory? Explanation is given by the fact, that both exchange and correlation energies have slightly differently meanings in the Hartree-Fock and DFT theories, thus direct substitution of Hartree-Fock exchange energy into the DFT energy functional would not give the desired results.

one of the most widely used computational methods in atomistic scale simulations [55].

2.2 Force field methods

2.2.1 Internal coordinates

For the sake of human readability a basis set defined by the local geometry is introduced when describing systems at atomistic scale. In crystalline systems the primitive vectors of the Bravais lattice are used. Considering molecular structures the so-called internal coordinates – bond length, valence angle and dihedral angle – are commonly applied. The first two are rather self explanatory. Bond length is defined by to covalently bonded atoms and the valence angle by three sequentially bonded atoms. Dihedral angle – also known as torsion angle – on the other hand is constructed using four atoms, such that when looking in the direction define by the middle atoms, the angle Φ forms between the two outer atoms. Fig. 2.1 illustrates the internal coordinates.

(a) Bond length r_{ij}

(b) Valence angle θ

(c)

(d) Dihedral angle Φ
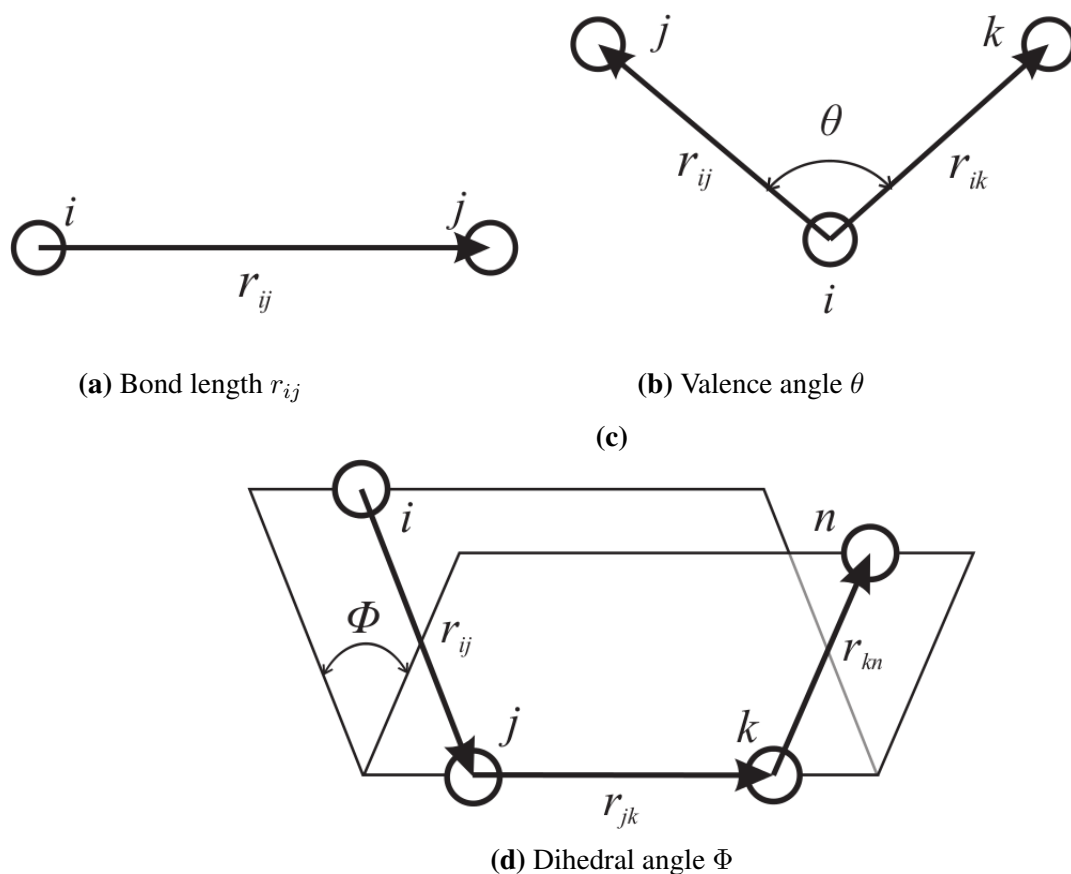
Figure 2.1: Internal coordinates [57]

2.2.2 The force fields

Force field methods rely on the assumption that the potential energy surface determined by the electronic Schrödinger equation can be sufficiently approximated via combinations of classical potentials[2] as functions of the positions of nuclei. A full set of these potentials for a specific system is called the "force field" (FF). The exact form of the FF depends on the nature of the system being simulated. For molecular system, such as investigated in the present theses, it is common to tie the FF with the internal degrees of freedom represented by the internal coordinates

$$U_{FF} = \underbrace{U_{bond\_stretch} + U_{angle\_bend} + U_{dihedral\_rotation}}_{\Delta E \text{ associated with change of internal coordinates}} + \underbrace{U_{VDW} + U_{Coulomb}}_{\substack{\text{van der Waals and} \\ \text{Coulomb interactions}}} + \ldots \quad . \quad (2.7)$$

In addition to the components shown in (2.7) extra terms can be added to fine-tune the FF for some specific purpose. In simulations conducted in this thesis only the five primary terms shown above are used. These potentials can be determined by fitting either experimental or quantum mechanical calculation results to some analytical function. Bond and valence angle potentials are usually described as harmonic oscillators, giving a rather good approximation in the vicinity of energy minimum. As the dihedral angle potentials should be invariant to full rotations, these are most often represented as combinations of periodic functions. The most common forms for Van der Waals interactions are the Lennard-Jones (2.8) and Morse (2.9) potential, where r_0. ϵ and σ are considered fitted parameters in the MD framework. Coulomb interaction is in its usual form and the atomic charges are calculated from quantum mechanical methods.

$$U_{LJ}(r) = \epsilon \left[\left(\frac{r_0}{r} \right)^{12} - 2 \left(\frac{r_0}{r} \right)^6 \right] \tag{2.8}$$

$$U_{Morse}(r) = \epsilon \left[\left(1 - e^{-\frac{r-r_0}{\sigma}} \right)^2 - 1 \right] \tag{2.9}$$

Both van der Waals and Coulomb interactions are taken as long-range interaction, which are only calculated between atoms that are not connected via bond, angle or dihedral potentials, because their effect has already been included in the potentials for internal coordinates.

---

[2]In MD literature "potential" is usually meant as exactly synonymous to potential energy. Throughout this thesis the same approach is applied.

2.2.3 Classical molecular dynamics (MD)

In MD simulations the time evolution of atomistic systems in a potentials defined by a force field are calculated by integrating the Newtonian equations of motion (2.10) over discrete time intervals Δt. As a result, the trajectories for whole systems are produced via periodic printing of the current positions of atoms over a fixed time period. Relying on the ergodic hypothesis, the physical observables are evaluated by averaging over time, ensemble or both, dependent on the nature of the phenomena. In this context an ensemble is meant as a set of atoms similar in regards to the quantity calculated.

$$m_i \frac{d}{dt}\vec{r}_i\left(t\right) = \vec{F}_i\left(\vec{r}_i\left(t\right)\right) = \nabla U_{FFi}\left(\vec{r}\left(t\right)\right), \qquad i = 1 \ldots N \qquad (2.10)$$

Considering statistical mechanics, ensembles are also meant as more generally representing the whole system and its' parameters. The microcanonical ensemble for example, is a fixed set of particles with a controlled volume and total energy, thus being abbreviated NVE. Temperatures are experimentally much easier to maintain than energies. Thus implementing the canonical ensemble NVT is more frequent. Additionally, constraining the volume is often impossible or dangerous, and a more sensible solution would be to apply constant pressure. Therefore, it is most common to replicate the experimental environment with the isothermal-isobaric ensemble NPT.

Control over temperature and pressure is retained using some specific thermostat or barostat algorithm correspondingly. The conceptual idea is to introduce some fictitious environmental forces, such that the analytic formation of NVT and NPT distribution functions would be reproduced as best as possible. Constant volumes can be maintained by implementing a simulation box with specific geometry and boundary conditions. Periodic boundaries are one of the most common, as they allow to avoid unwanted surface phenomena and model bulk materials. As long-range interactions have a sharp distance dependence, it's reasonable to calculated them only within a defined cutoff radius. Especially when applying periodic boundaries, where a cut-off less than half of the smallest box dimension is required to avoid infinite loops.

Describing the time evolution implies usage of a numeric integrator. Naturally, only algorithms introducing small fluctuations around the exact, rather that drifting of results, are suitable. Ensuing from physical considerations additional symmetry properties are demanded. As the Newtonian equations of motion are time-reversible, so should the integrator be. Liouville's theorem must be applicable – the integrator has to conserve phase space volume. Furthermore, symplecticity i required. The last is essentially a generalization of the Liouville's theorem:

phase space volumes enclosed by areas defined by pairs of canonical variables, have to be conserved. The Verlet type integrators are an example of satisfying all of these.

In the present work the *leapfrog* Verlet [57] algorithm is used. The name stems from the fact, that velocities $\vec{v}$ half a time-step $\frac{1}{2}\Delta t$ out of phase with the positions $\vec{r}$ and forces $\vec{F}$ are used. The essential scheme is:

1. a "leap" is made for the velocities, using forces half a time-step in advance

$$\vec{v}\left(t - \frac{1}{2}\Delta t\right) + \Delta t \frac{\vec{F}(\vec{r}(t))}{m} = \vec{v}\left(t + \frac{1}{2}\Delta t\right) \tag{2.11}$$

2. using the new velocities a "leap" is made for the positions

$$\vec{r}(t) + \Delta t \vec{v}\left(t + \frac{1}{2}\Delta t\right) = \vec{r}(t + \Delta t). \tag{2.12}$$

This is continued until reaching a predefined end condition, usually in the form of maximum number on time-steps. Physical observable, which require the usage of velocities and positions at the same time, are calculated by

$$\vec{v}(t) = \frac{\vec{v}\left(t - \frac{1}{2}\Delta t\right) + \vec{v}\left(t + \frac{1}{2}\Delta t\right)}{2}. \tag{2.13}$$

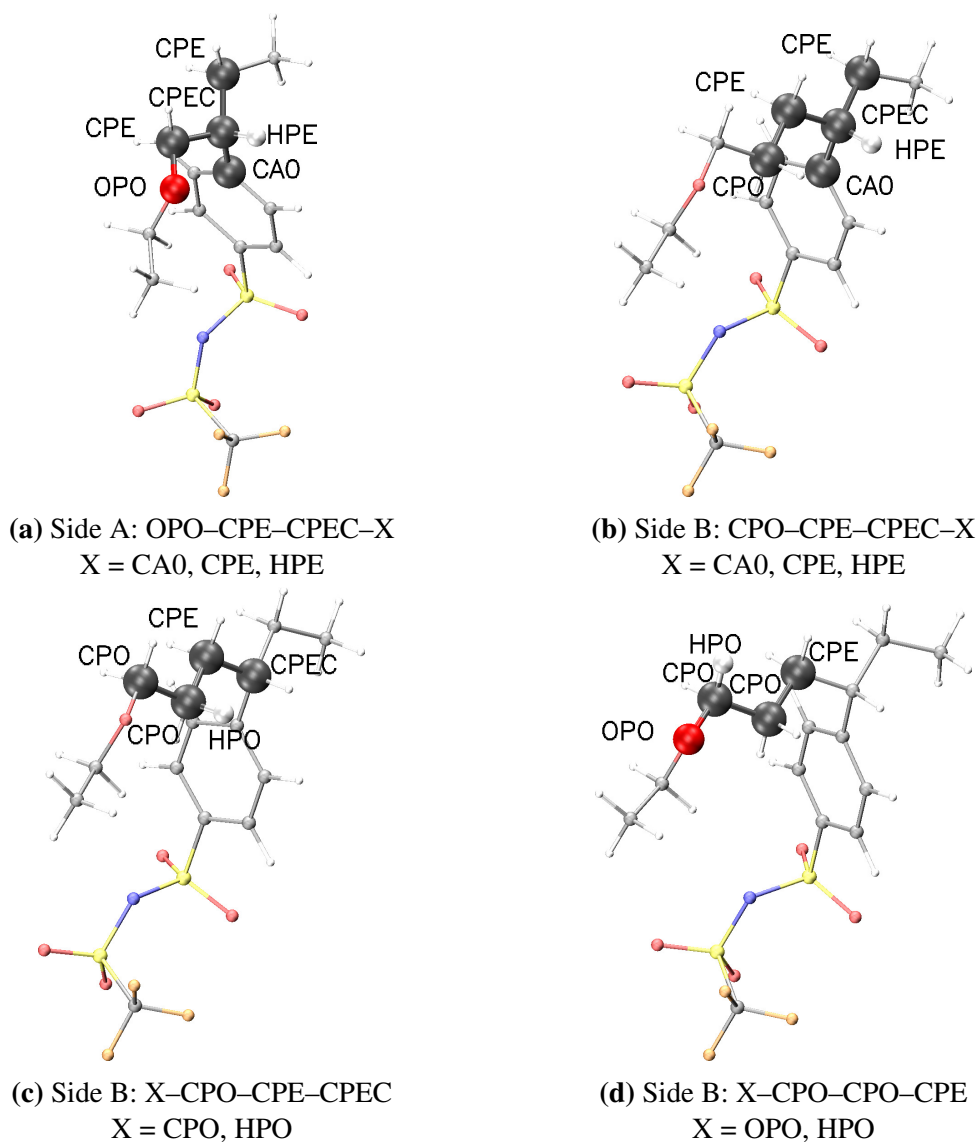# Chapter 3

Simulations and analysis

3.1 Force field

Eq. (3.1) shows the basic force field structure used. Systems containing PEO, P(STFSILi) or both have been previously simulated using MD [39, 41, 44]. Therefore most of the force field was combined from published [39, 41, 44, 47–51] articles. Additionally, density functional theory calculations of ten dihedral angle potentials for PEO and P(STFSILi) connection sites were carried out in the present work. Details for force field parameters not calculated in this theses can be found from [44].

$$U_{FF} = U_{bond\_stretch} + U_{angle\_bend} + U_{dihedral\_rotation} + U_{VDW} + U_{Coulumb} \qquad (3.1)$$

It is also noteworthy the Li$^+$ was described only with Coulomb and van der Waals interaction, thus making dissociation possible in the force field framework.

3.1.1 Dihedral potential calculations

For consistency considerations the same level of theory – hybrid functional B3LYP [58] with split valence basis set 6-31+G(d,p) – was used as in [44] for P(STFSILi) force field development. Calculations were preformed with *Gaussian 03* [59] software. In order to keep in the limit of accessible computational resources, the smallest possible representative systems were chosen. As the PEO repetitive unit (see Fig. 1.1b) is not symmetric, the connection sites on both sides differed by two $-CH2-$ units. Fig. 3.1a highlights dihedral angles calculated on side A and Fig. 3.1b to 3.1d highlights those calculated for side B. First, both of the geometries

(a) Side A: OPO–CPE–CPEC–X
X = CA0, CPE, HPE

(b) Side B: CPO–CPE–CPEC–X
X = CA0, CPE, HPE

(c) Side B: X–CPO–CPE–CPEC
X = CPO, HPO

(d) Side B: X–CPO–CPO–CPE
X = OPO, HPO

Figure 3.1: The dihedral angles for which potentials were calculate

(side A and B) were optimized. Followed by scanning the PES with $2.5°$ dihedral angles steps, while holding the rest of the geometry fixed. As expected, the resulting potential energy plots were periodic over $360°$ and angles which shared two middle atoms only differed from each other by a phase difference. The potentials were fitted against Fourier series up to the eighth term

$$U(\theta) = A_0 + \sum_{n=1}^{7} A_n \cos\left(n\theta - \phi_n\right). \tag{3.2}$$

A sample of the results is provided on Fig. 3.2, full set of the dihedral angle potentials developed is found with in appendix A.
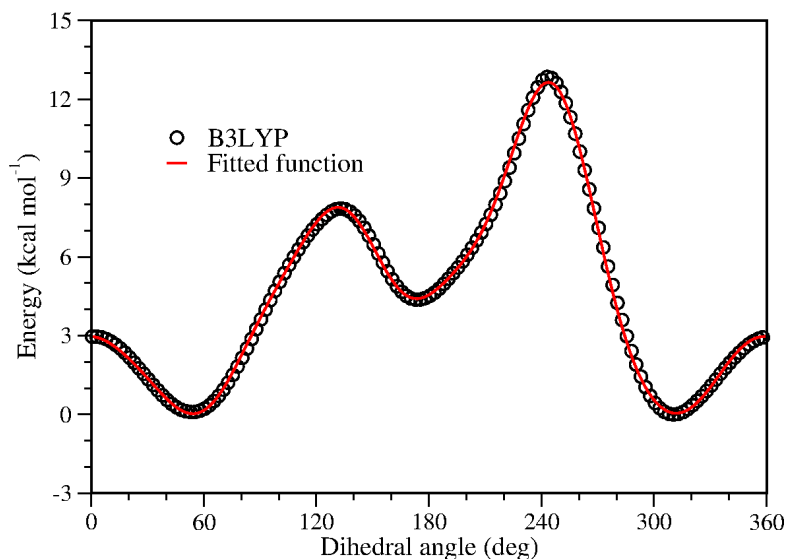
Figure 3.2: A sample of dihedral angle potential: X–CPE–CPEC–Y

3.2 Initial configurations

Five structures with the empirical formula $P(STFSILi)_p-PEO_n-P(STFSILi)_p$ were generated. Corresponding to the polymers synthesized by Bouchet *et al.* [20] the length of the PEO chain was always $n = 796$, while the P(STFSILi) chains variated such that $p = \{6, 11, 15, 24, 41\}$. Table 1.1 lists the simulated and corresponding experimental polymers and Fig. 1.1 illustrates their repetitive units. The equilibrium bond length, valence and dihedral angle values were determined by the force field. To replicate an amorphous PEO chain the OPO−CPO−CPO−OPO and CPO−CPO−OPO−CPO (see Fig. 1.1b) dihedral angels were randomly generated using a locally developed Monte Carlo software *mcgen* [60]. For all chain lengths twelve single molecule systems were generated with different random seeds. From these the one with the lowest energy was chosen for all $p = \{6, 11, 15, 24, 41\}$. Reproduction of bulk environment was implemented via the periodic boundary conditions. As an example, Fig. 3.3 visualizes the BAB24 initial structure generated with *mcgen* and how it is packed into the simulation box.

3.3 MD simulations

The DL_POLY_2 [61, 62] software was used for all MD simulations. Integration was implemented with the leapfrog Verlet [57] method with a $0.5\,fs$ time-step. Sampling was made every $0.5\,ps$ (every 1000 time-step). Periodic boundary condition were applied in all three dimensions of the cubic simulation box. To ease the initial configuration generation, the

starting volumes were defined significantly larger than the experimental PEO density would suggest, ranging from 60^3 to 75^3 Å^3. During annealing these shrank down to 38^3–42^3 Å^3. Nosé-Hoover [63] thermostat was used for NVT and the Melchionna [64] algorithm of combining the Nosé-Hoover thermostat with a barostat for NPT [57]. The corresponding relaxation times for the termostat and the barostat were 0.1 and 0.3 ps.

First, all systems were equilibrated for 2.5 ns with NVT ensemble at 293 K to get rid of possible tensions. Next, adequately uniform polymer distribution was ensured by fast simulated annealing:

1. stepwise heating with 10 ps NPT runs and 100 K steps from 400 up to 900 K

2. 100 ps relaxation at 1000 K

3. stepwise cooling with 25 ps runs and 100 K steps from 900 back down to 400 K

The relaxation procedure and periodic boundary conditions are illustrated in Fig. 3.3. Finally, the polymers were allowed to evolve in local equilibrium with NPT ensemble for 10 ns at eight temperatures form 293 to 363 K with 10 K step. This last simulation step was sampled for analyzes.

3.4   Analysis methods
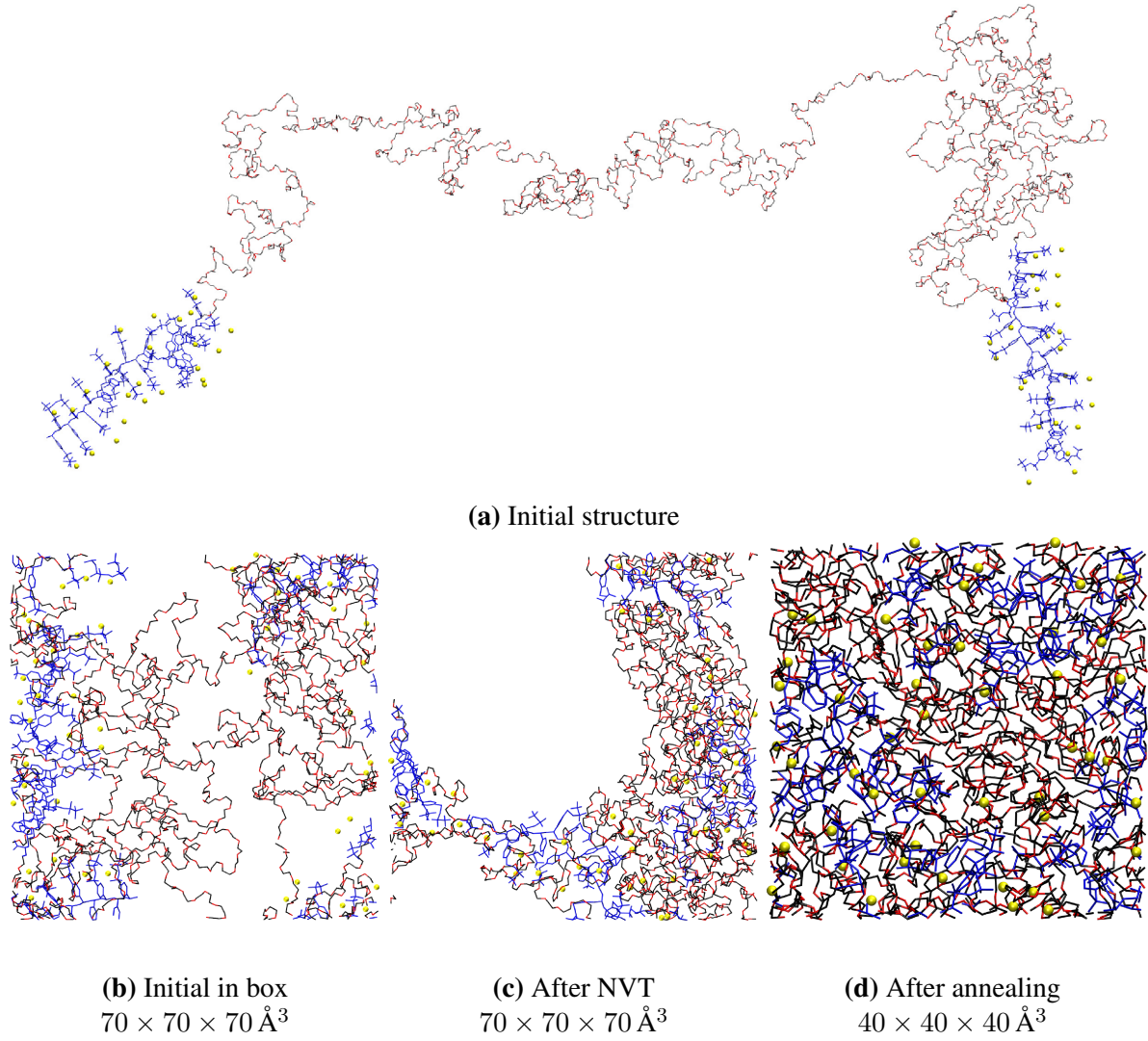
3.4.1   Dynamics

System dynamics can be analyzed by the mean square displacement (MSD) calculated as a function of time

$$MSD(t) = \left\langle [\Delta \vec{r}(t)]^2 \right\rangle = \left\langle [\vec{r}(t) - \vec{r}(0)]^2 \right\rangle \tag{3.3}$$

where $\vec{r}(t)$ is the position vector of a given atom. The averaging is done over time and atom type. From the MSD the self-diffusion coefficient (SDC) $D(t)$ can be expressed

$$D(t) = \frac{1}{2n} \lim_{t \to \infty} \frac{MSD(t)}{t}, \tag{3.4}$$

where n is the dimension of the observed space. In this work a three dimensional ($n = 3$) case was studied. Although simulations are always conducted in finite timescales, it is common [35, 44, 65] to use Eq. (3.4) to evaluate the relative diffusive properties. Li$^+$ self-diffusion can be

(a) Initial structure

| **(b)** Initial in box | **(c)** After NVT | **(d)** After annealing |
| $70 \times 70 \times 70 \,\text{Å}^3$ | $70 \times 70 \times 70 \,\text{Å}^3$ | $40 \times 40 \times 40 \,\text{Å}^3$ |

Figure 3.3: structure of BAB24 generated with *mcgen* (a) and during phases of the relaxation procedure (b),(c),(d); PEO – red and black, P(STFSI$^-$) – blue, Li$^+$ – yellow

taken as a measure of the polymer conductivity [65] using the Nernst-Einstein equation

$$\Lambda = \frac{\alpha N e^2 \left(D_+ + D_-\right)}{V k_b T},$$
(3.5)

where N is the total number of ions in the simulation box, e the elementary charge, α the degree of uncorrelated ion motion typically measured as the ratio of total charge transport to the diffusive charge transport, V the simulation box volume, k_b the Boltzman constant, T temperature and $D_{+/-}$ cation and anion SDC correspondingly.

The MSD(t) plots are in a good approximation linear, thus the SDC is essentially an evaluation of MSD(t) slopes. Therefore, it is convenient to ignore, that "diffusion" of a polymer chain inside itself is a dubious concept, and use "SDC" to evaluate and compare the thermal motion

of different parts of the polymer.

3.4.2 Structure

Structural properties can be analyzed by calculating the radial distribution function (RDF)

$$g(r)_{AB} = 4\pi r^2 \rho(r)_{AB} dr, \tag{3.6}$$

where $\rho_{AB}(r)$ is the number density of B-type atoms in the distance r from A-type atoms. RDF gives the probability of finding an B-type atom in the distance r from an A-type atom. The values are averaged over time and the ensemble of AB pairs. Integrating $g(r)_{AB}$ over r gives the coordination number function (CN) for the pair AB. This shows how many B-type atoms neighbor the A-type atom on average.

The radius of gyration R_g describes the dimensions of the polymer chain:

$$R_g = \sqrt{\frac{1}{N} \sum_{k=1}^{N} (\vec{r}_k - \vec{r}_0)^2}, \tag{3.7}$$

where $\vec{r}_k$ is the position of kth atom and $\vec{r}_0$ the position of the central monomer of the chain. When calculating the radius of gyration, the molecule is unpacked from the periodic boundary box. Additionally the mass density of the simulation box can be calculated to evaluate the free space in the system.

Chapter 4

Results and discussion

Considering the structural properties of the simulated polymers, it is evident from the radial distribution functions (RDF), that Li^+ is fully dissolved by the PEO matrix. Both in NVT and NPT runs Li^+–O_{PEO} RDF has a sharp peak at $1.9\ldots2.0$ Å. This is in good correspondence with previous studies [36]. In the production runs, Li^+ gives significant RDF peaks only with PEO oxygen. The P(STFSILi) oxygens also indicate considerable RDF peaks with Li^+ in the initial NVT relaxation runs, however these are 2–6 times smaller than those with O_{PEO}. Both RDFs and coordination numbers (CN) are effectively constant over the simulated temperature range. Characteristic results are presented in Fig. 4.1.
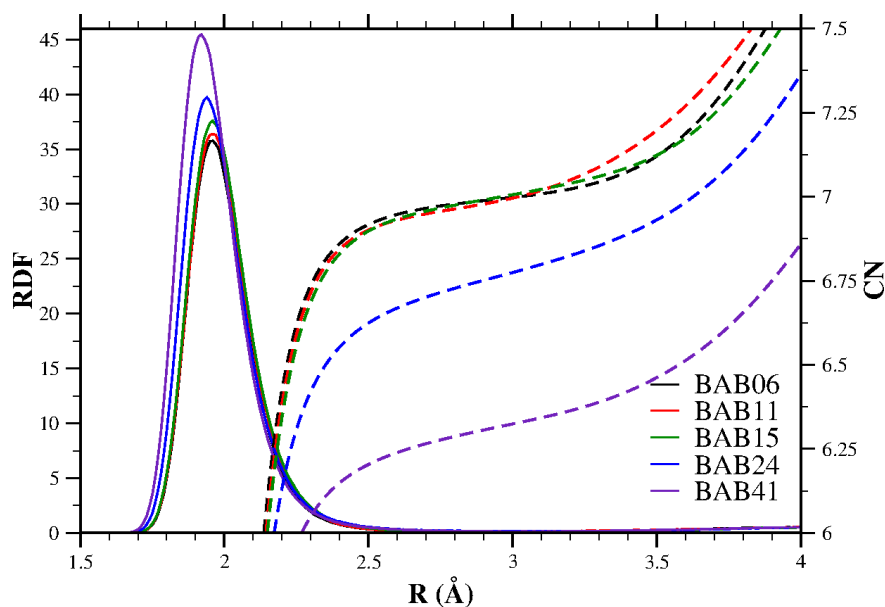
Figure 4.1: Li^+ – O_{PEO} RDF and CN at 293 K (NPT)

Li$^+$ is coordinates to 6–7 PEO oxygen atoms (Fig. 4.1), as was also shown in a previous study of similar systems using the force field [44]. This varies from the commonly accepted 5–6 [36]. Thus, conclusions about the specific mechanisms of ion conduction should not be made from these simulations. Nevertheless, as the main concepts of Li$^+$ being coordinated with PEO oxygens and conducted via the PEO chain motion are reflected reliably, qualitative description of both temperature and chain length dependencies can still be considered valid. A characteristic Li$^+$–PEO interaction for the three shorter P(STFSILi) chain lengths is shown in Fig. 4.2. The irregular values of distances between Li$^+$ and O indicate a dynamic situation.
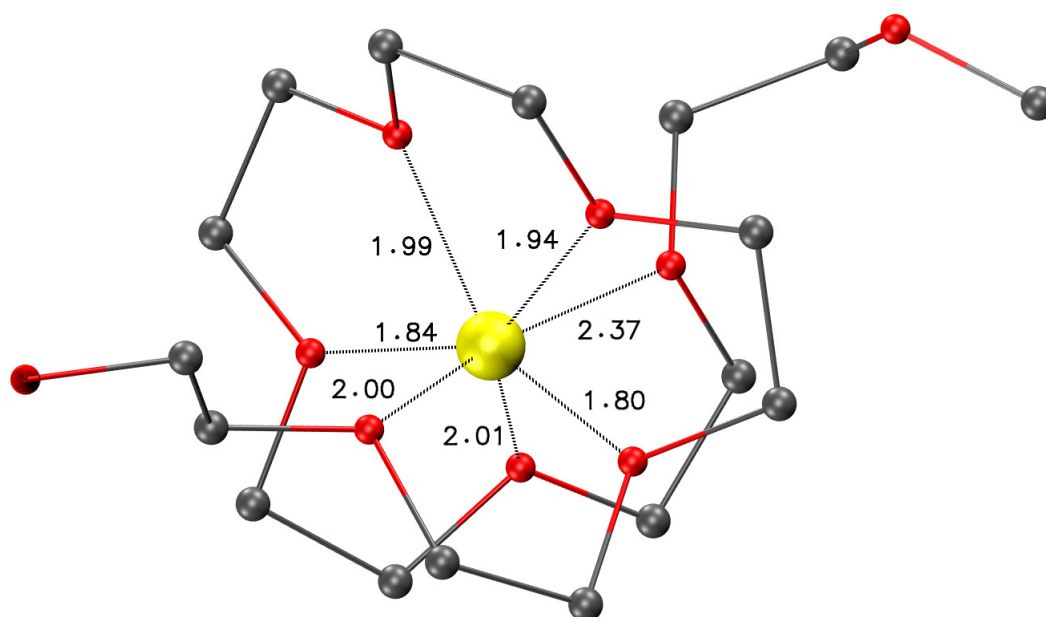

Figure 4.2: A typical example of Li$^+$ coordinated to PEO oxygens
Li$^+$ – yellow, O – red, C – grey

The self-diffusion coefficients (SDC) for Li$^+$ and PEO oxygen can be seen in Fig. 4.3. Different columns correspond to different chain lengths and colors to temperatures. The dotted lines are meant only as guidelines for the eyes. There is clearly an observable change of temperature sensitivity accompanying the chain length variation. Polymers with lower [Li$^+$]:[O] ratio show a much faster growth of SDC with temperature rising. For the two largest polymers, BAB24 and BAB41, the SDC varies little with temperature change. Also it is evident, that larger polymers have a significantly lower SDC. In principle, the SDC follows an exponential-like curve. Edman *et al.* [45] have experimentally shown this trend also to apply for a similar system of PEO doped with LiN(SO$_2$CF$_3$)$_2$ salts.

The disorder in SDC temperature and P(STFSILi) chain length dependences can be explained by the Li$^+$ or the polymer chain itself being geometrically locked between the polymer segments. Due to the more rigid structure of P(STFSILi), it is more prone to such trapping
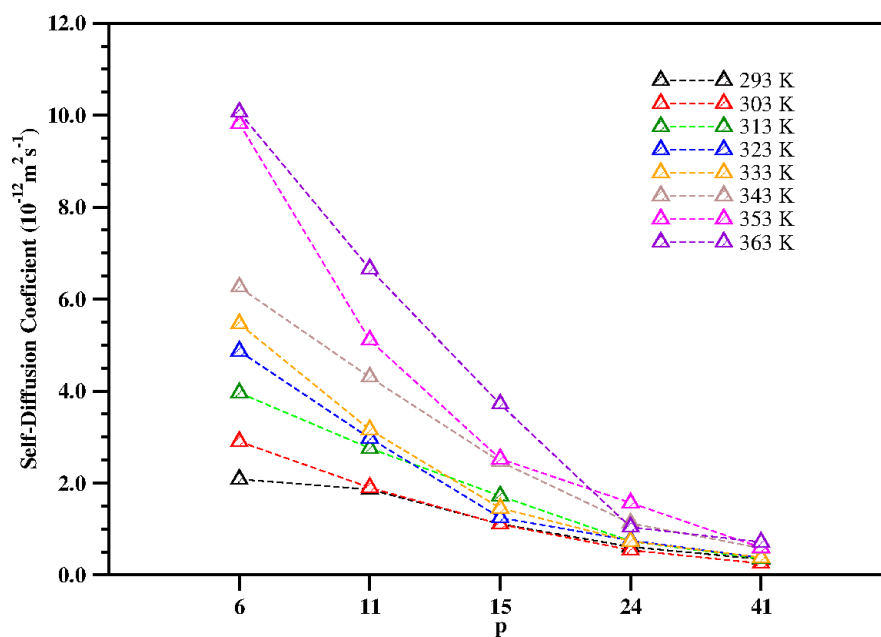
(a) PEO oxygen
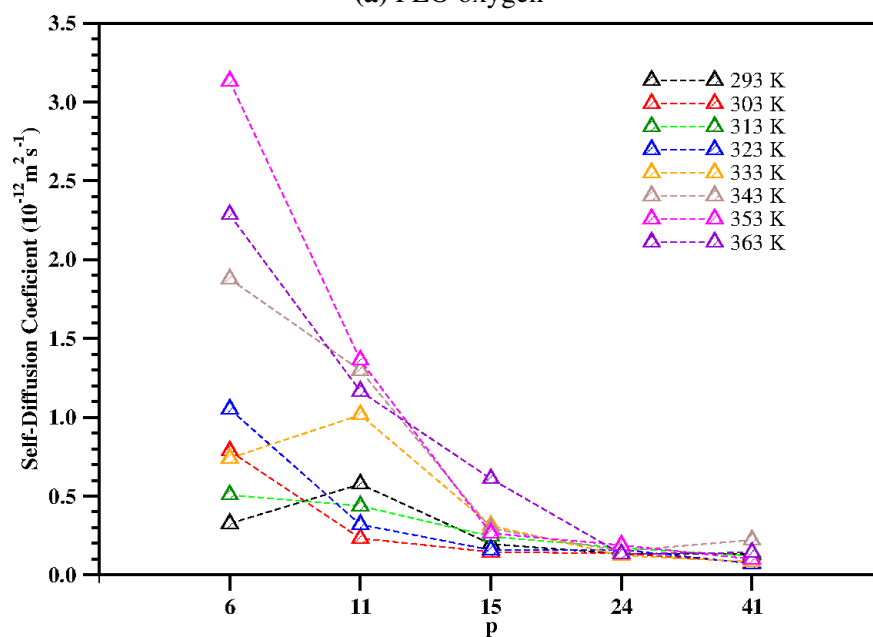
(b) Li$^+$

Figure 4.3: SDC of PEO oxygen and Li$^+$

(Fig. 4.4). Unfortunately due to computational limitations, the sample size is not large enough to average this out. Also it can be seen, that for both PEO and Li$^+$ there is an abnormal SDC rise at 353 K. This is further illustrated by Fig. 4.4, which shows the SDC for the terminal and chain carbons of P(STFSILi). The phenomena is especially strong for the chain carbons of BAB06 and BAB11. The experimental differential scanning calorimetry [20] thermograms indicate that polymers with shorter P(STFSILi) chains have melting temperatures around 40–60 °C.
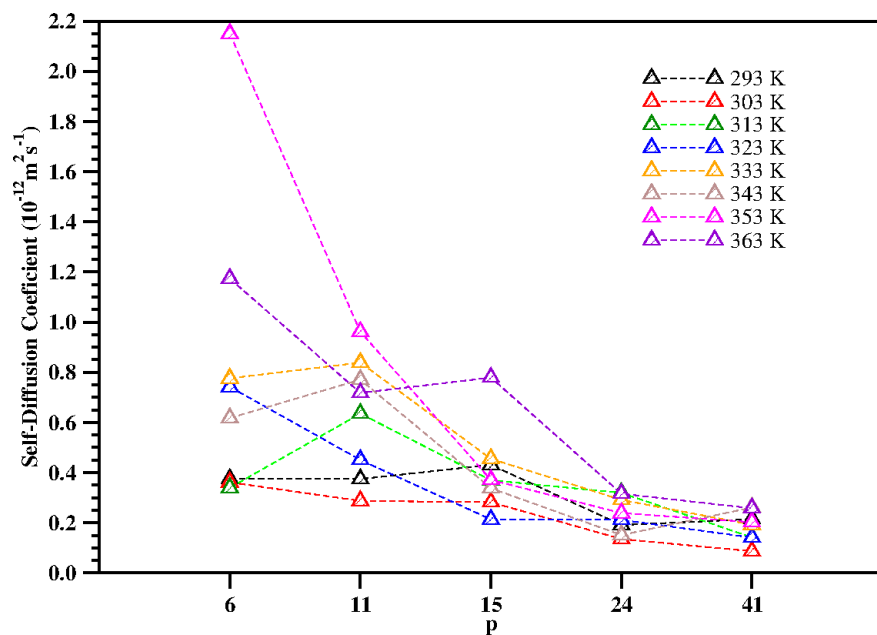
(a) CT
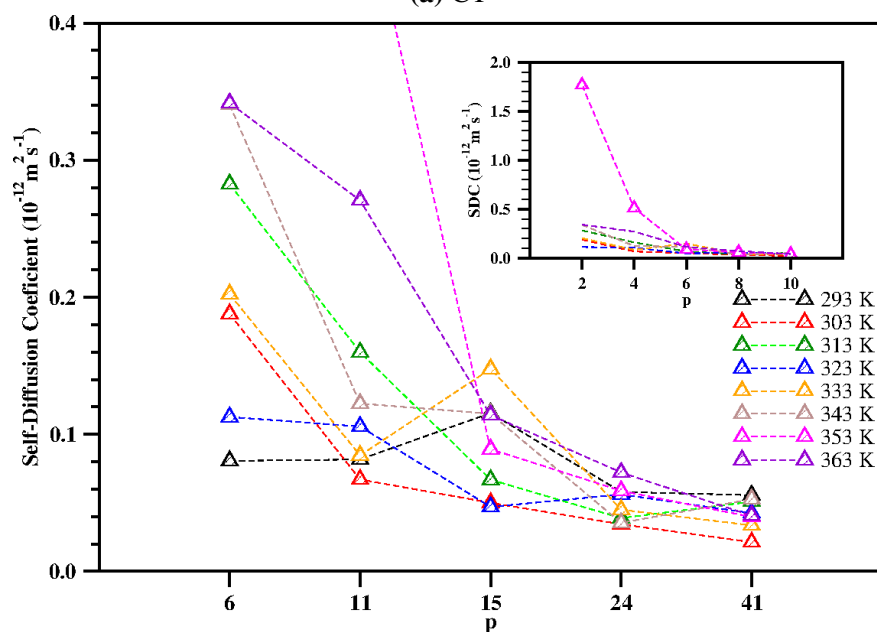
(b) CPEC

Figure 4.4: SDC of P(STFISILi) terminal (CT) and chain (CPEC) carbons

Therefore, the anomalous behavior at $353\,\text{K}$ could be a reflection of the melting, with a wrong temperature due to the incapability of the force field to replicate phase transition reliably.

As demonstrated in Fig. 4.4, the SDC differs quite a lot along the styrene-TFSILi block. Expectedly the SDC increases with distance from the main polymer chain. The terminal carbons actually show only slightly lower SDC values than Li$^+$. On the other hand, the chain carbons have about an order of magnitude smaller SDC. This could hint at a possible reason for

the temperature dependence decrease with the growth of [Li$^+$]:[O] ratios. Compared to PEO the P(STFSILi) has a relatively rigid and large repetitive unit. Considering the small variation in final simulation box sizes (38^3–42^3 Å^3), it could be reasoned that the total volume of the polymers was mostly defined by PEO. Due to its amorphous state, the latter could effectively pack around the P(STFSILi), which is illustrated in Fig. 3.3. This is also supported by the relative densities provided in Fig. 4.5. It is reasonable to propose, that the insertion of these stiff and bulky structures introduces geometrical constraints on the PEO chain motion, impairing the diffusion phenomena.
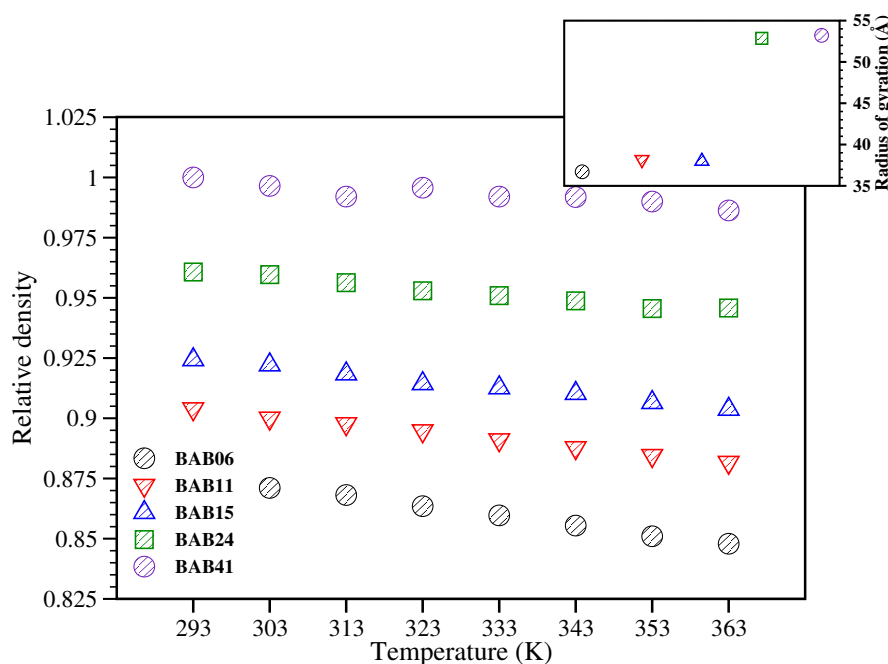
Figure 4.5: Relative densities and averaged radii of gyration

Values of the radii of gyration R_g (right corner of Fig. 4.5) display a fascinating characteristic. Changes in P(STFSILi) chain lengths hardly alter the R_g, except for a sharp jump of nearly 40% between BAB15 and BAB24. This has a few indications. First, there probably exists a critical P(STFSILi) chain length in the range of 15–24. Secondly, the nearly constant plateaus further support the concept of the total volume being mostly determined by PEO. Finally, a question is risen by the lack of a corresponding jump in the densities or total volumes. This might be a feature of the material, simulation setup or both.

Usage of periodic boundaries could possibly introduce artificial bulk conditions. Furthermore, in the current simulations, systematic structural composition was limited to the monomer internal geometries and sequential order. On higher levels the material was modeled as a uniform mesh of mostly random conformations. It is highly probable that morphology effects play a significant rôle in determining the polymer properties. But due to the lack of

experimental specifications, the simplest case was applied in the present work. Thus guidelines for further research are emergent: (a) probe the P(STFSILi) chain lengths in the range of 15–24, (b) check for possible methodical artefacts and (c) study effects of higher level structural properties.

Summary

Industrial scale implementations of solid polymer electrolyte batteries could potentially revolutionize the energy storage market and usher an era of electric vehicles. However, first materials with sufficiently high ionic conductivity and mechanical strength must be developed. Advancement could be enhance by insight into the fundamental concepts determining the materials properties.

With this in mind, the aim of the present thesis was to probe the molecular level phenomena in a novel family of single-ion BAB triblock copolymer electrolytes $P(STFSILi)_p-PEO_n-P(STFSILi)_p$, recently reported by Bouchet *et al.* [20]. Specifically the temperature and P(STFSILi) chain length dependence was investigated by classical molecular dynamics (MD) simulations.

Most of the force field, necessary for MD, was compiled from published works [39, 41, 44, 47–51]. Additionally, several dihedral angle potentials were calculated from density functional theory implementing the hybrid functional B3LYP [58] with split valence basis set 6-31+G(d,p).

The self-diffusion coefficients (SDC), calculated form the mean square displacements, were analyzed as model measures of both Li^+ conductivity and the thermal motions of different polymer parts. The SDCs demonstrated a strong exponential-like decrease with growth of the P(STFSILi) chain length. Additionally it is observed, that polymers with higher $[Li^+]$:[O] ratios have a smaller SDC temperature dependence.

Relaying on the system density growth with P(STFSILi) chain length, it is proposed that above mentioned exponential-like behavior is due to increase of geometrical constrains on PEO motion. Furthermore, based on the step-function-like behavior of the radii of gyration, a critical P(STFSILi) chain length value is hypothesized to be found in the range of 15–24.

Mono-ioonse BAB-kolmikplokk kopolümeerelektrolüüdi omaduste uurimine arvutisimulatsioonidega

Madis Ollikainen

Kokkuvõte

Tööstuslikus mastaabis rakendatava tahkispolümeeraku väljatöötamine võiks potentsiaalselt võimaldada laialdast elektriautode kasutusele võttu. Hetkeseisuga ei leidu aga sobivat elektrolüüdimaterjali, milles oleksid kombineeritud kõrge ioon-juhtivus ja mehaaniline tugevus. Eksperimentaalse arendustöö kiirendamiseks oleks tarvilik laiendada teadmisi materjalide omadusi määravatest fundamentaalsetest nähtustest.

Eelnevast lähtudes on käesolevas töös uuritud hiljuti Bouchet *et al.* [20] sünteesitud mono-ioonse BAB-kolmikplokk kopolümeerelektrolüüdi $P(STFSILi)_p - PEO_n - P(STFSILi)_p$ juhtivuslike omaduste sõltuvust temperatuurist ja P(STFSILi) ahela pikkusest. Töö läbiviimiseks on valitud klassikalise molekulaardünaamilise simulatsiooni meetod, mis võimaldab kirjeldada süsteemi atomaarsel tasandil. Aatomitevahelisi interaktsioone kirjeldavate potentsiaalide kogum ehk *jõuväli* on suuremas osas kompileeritud varasemalt publitseeritud töödest [39, 41, 44, 47–51]. Lisaks arvutati mõningaste kahetahuliste nurkade potentsiaalid kasutasutades thedusfunktsionaali teooriat hübriidfunktsionaaliga B3LYP [58] lõhestatud baasil 6-31+G(d,p).

Nii Li^+ juhtivust kui ka polümeeriahela liikuvust saab hinnata, arvutades simulatsioonidest aatomite enesedifusioonikoefitsendid. Viimastel esineb tugev sõltuvus $[Li^+]:[O]$ suhtest, kahanedes eksponentsiaalselt $[Li^+]:[O]$ kasvades. Täheldatav on ka difusioonikoefitsentide temperatuuritundlikkuse märkimisväärne alanemine $[Li^+]:[O]$ kasvades. Toetudes asjaolule, et P(STFSILi) ahelate pikenedes süsteemi tihedus kasvas, võib teha järelduse polümeeriahela liikuvust piiravate geomeetriliste tegurite võimendumisest $[Li^+]:[O]$ suurenedes. Seda nähtust pakutakse seletuseks eeltoodud eksponentsiaalsele sõltuvusele.

Polümeeride güratsiooniraadiustel täheldatakse tähelepanuväärset astmefunktsioonikujulist profiili. Järsk muutus polümeeriahela sirutusulatuses viitab, et P(STFSILi) ahelapikkuste vahemikus 15–24 paikneb ilmselt kriitiline ahelapikkus.

Acknowledgement

Bibliography

[1] Jeff Tollefson. Car industry: Charging up the future. *Nature*, 456(November):436–440, 2008.

[2] M Armand and J-M Tarascon. Building better batteries. *Nature*, 451(7179):652–7, February 2008.

[3] Richard van Noorden. A better battery. *Nature*, 507(March):26–28, 2014.

[4] J M Tarascon and M Armand. Issues and challenges facing rechargeable lithium batteries. *Nature*, 414(6861):359–67, November 2001.

[5] Fangyi Cheng, Jing Liang, Zhanliang Tao, and Jun Chen. Functional materials for rechargeable batteries. *Advanced materials (Deerfield Beach, Fla.)*, 23(15):1695–715, April 2011.

[6] Peter G Bruce, Stefan a Freunberger, Laurence J Hardwick, and Jean-Marie Tarascon. Li-O2 and Li-S batteries with high energy storage. *Nature materials*, 11(1):19–29, January 2012.

[7] Wen-Shiue Young, Wei-Fan Kuan, and Thomas H. Epps. Block copolymer electrolytes for rechargeable lithium batteries. *Journal of Polymer Science Part B: Polymer Physics*, 52(1):1–16, January 2014.

[8] Kazuo Murata, Shuichi Izuchi, and Youetsu Yoshihisa. An overview of the research and development of solid polymer electrolyte batteries. *Electrochimica Acta*, 45(8-9):1501–1508, January 2000.

[9] C Brissot, M Rosso, J.-N Chazalviel, P Baudry, and S Lascaud. In situ study of dendritic growth inlithium/PEO-salt/lithium cells. *Electrochimica Acta*, 43(10-11):1569–1574, April 1998.

[10] Michel Rosso, Claire Brissot, Anna Teyssot, Mickaël Dollé, Lucas Sannier, Jean-Marie

Tarascon, Renaud Bouchet, and Stéphane Lascaud. Dendrite short-circuit and fuse effect on Li/polymer/Li cells. *Electrochimica Acta*, 51(25):5334–5340, July 2006.

[11] Charles Monroe and John Newman. The Impact of Elastic Deformation on Deposition Kinetics at Lithium/Polymer Interfaces. *Journal of The Electrochemical Society*, 152(2):A396, 2005.

[12] Philippe Poizot and Franck Dolhem. Clean energy new deal for a sustainable world: from non-CO2 generating energy sources to greener electrochemical storage devices. *Energy & Environmental Science*, 4(6):2003, 2011.

[13] Vito Di Noto, Sandra Lavina, Guinevere a. Giffin, Enrico Negro, and Bruno Scrosati. Polymer electrolytes: Present, past and future. *Electrochimica Acta*, 57:4–13, December 2011.

[14] Myounggu Park, Xiangchun Zhang, Myoungdo Chung, Gregory B. Less, and Ann Marie Sastry. A review of conduction phenomena in Li-ion batteries. *Journal of Power Sources*, 195(24):7904–7929, December 2010.

[15] P. G. Bruce and C. a. Vincent. Polymer electrolytes. *Journal of the Chemical Society, Faraday Transactions*, 89(17):3187, 1993.

[16] Tianran Zhang, Daixin Li, Zhanliang Tao, and Jun Chen. Understanding electrode materials of rechargeable lithium batteries via DFT calculations. *Progress in Natural Science: Materials International*, 23(3):256–272, June 2013.

[17] Li-Tang Yan and Xu-Ming Xie. Computational modeling and simulation of nanoparticle self-assembly in polymeric systems: Structures, properties and external field effects. *Progress in Polymer Science*, 38(2):369–405, February 2013.

[18] Gerbrand Ceder. Opportunities and challenges for fi rst-principles materials design and applications to Li battery materials. *MRS Bulletin*, 35(September):693–702, 2010.

[19] Ellad B. Tadmor and Ronald E. Miller. *Modeling Materials: Continuum, Atomistic and Multiscale Techniques*. Cambridge University Press, Cambridge, 2011.

[20] Renaud Bouchet, Sébastien Maria, Rachid Meziane, Abdelmaula Aboulaich, Livie Lienafa, Jean-pierre Bonnet, Trang N T Phan, Denis Bertin, Didier Gigmes, Didier Devaux, Renaud Denoyel, and Michel Armand. Single-ion BAB triblock copolymers as highly efficient electrolytes for lithium-metal batteries. *Nature Materials*, 12(5):452–457, 2013.

[21] D.E. Fenton, J.M. Parker, and P.V. Wright. Complexes of alkali metal ions with poly(ethylene oxide). *Polymer*, 14(11):589, November 1973.

[22] Peter V Wright. Electrical conductivity in ionic complexes of poly(ethylene oxide). *British Polymer Journal*, 7(5):319–327, 1975.

[23] J M Chabagno M. Armand and M Duclot. Extended Abstract. *Second International Meeting on Solid Electrolytes, St Andrews, Scotland*, 1978.

[24] W H Meyer. Polymer electrolytes for lithium-ion batteries. *Advanced materials*, 10(6):439–48, April 1998.

[25] Eliana Quartarone and Piercarlo Mustarelli. Electrolytes for solid-state lithium rechargeable batteries: recent advances and perspectives. *Chemical Society reviews*, 40(5):2525–40, May 2011.

[26] R C Agrawal and G P Pandey. Solid polymer electrolytes: materials designing and all-solid-state battery applications: an overview. *Journal of Physics D: Applied Physics*, 41(22):223001, November 2008.

[27] Michel Armand. Polymer electrolytes. *Annual Review of Materials Science*, 16:245–261, 1986.

[28] Fiona M Gray. *Polymer Electrolytes*. The Royal Society of Chemistry, Cambridge, UK, 1997.

[29] Rachid Meziane, Jean-Pierre Bonnet, Matthieu Courty, Karim Djellab, and Michel Armand. Single-ion polymer electrolytes based on a delocalized polyanion for lithium batteries. *Electrochimica Acta*, 57:14–19, December 2011.

[30] J.-N. Chazalviel. Electrochemical aspects of the generation of ramified matallic electrodeposits. *Physical Review A*, 42(12):7355–7367, 1990.

[31] a Dobrynin and M Rubinstein. Theory of polyelectrolytes in solutions and at surfaces. *Progress in Polymer Science*, 30(11):1049–1118, November 2005.

[32] a. Manuel Stephan. Review on gel polymer electrolytes for lithium batteries. *European Polymer Journal*, 42(1):21–42, January 2006.

[33] C Berthier, W Gorecki, M Minier, M B Armand, J M Chabagno, and P Rigaud. IN ALKALI METAL SALTS-POLY (ETHYLENE OXIDE) ADDUClS. *Solid*, 11:91–95, 1983.

[34] Z Gadjourova, Y G Andreev, D P Tunstall, and P G Bruce. Ionic conductivity in crystalline polymer electrolytes. *Nature*, 412(6846):520–3, August 2001.

[35] Florian Muller-Plathe and Wilfred F. van Gunsteren. Computer simulation of a polymer electrolyte: Lithium iodide in amorphous poly(ethylene oxide). *The Journal of Chemical Physics*, 103(11):4745, 1995.

[36] Patrik Johansson, Jörgen Tegenfeldt, and Jan Lindgren. Modelling amorphous lithium salt–PEO polymer electrolytes: ab initio calculations of lithium ion–tetra-, penta- and hexaglyme complexes. *Polymer*, 40:4399–4406, July 1999.

[37] A. Liivat, D. Brandell, and J. O. Thomas. A molecular dynamics study of ion-conduction mechanisms in crystalline low-Mw LiPF6·PEO6. *Journal of Materials Chemistry*, 17(37):3938–3946, 2007.

[38] Grant D Smith, Richard L Jaffe, and Harry Partridge. Quantum Chemistry Study of the Interactions of Li+, Cl- and I- Ions with Model Ethers. *J. Phys. Chem. A*, 101:1705–1715, 1997.

[39] N Canongia Lopes and Blaise Pascal. Molecular Force Field for Ionic Liquids Composed of Triflate or Bistriflylimide Anions. *J. Phys. Chem. B*, 108:16893–16898, 2004.

[40] Oleg Borodin and Grant D Smith. Development of many-body polarizable force fields for Li-battery components: 1. Ether, alkane, and carbonate-based solvents. *The journal of physical chemistry. B*, 110(12):6279–92, March 2006.

[41] Sylvie Neyertz, David Brown, and John O. Thomas. Molecular dynamics simulation of crystalline poly(ethylene oxide). *The Journal of Chemical Physics*, 101(11):10064, 1994.

[42] Sylvie Neyertz and David Brown. A computer simulation study of the chain configurations in poly(ethylene oxide)-homolog melts. *The Journal of Chemical Physics*, 102(24):9725–9735, 1995.

[43] D. Brandell, A. Liivat, H. Kasemägi, A. Aabloo, and J. O. Thomas. Molecular dynamics simulation of the LiPF6PEO6 structure. *Journal of Materials Chemistry*, 15:1422–1428, 2005.

[44] Daniel Brandell, Heiki Kasemägi, Tarmo Tamm, and Alvo Aabloo. Molecular dynamics modeling the Li-PolystyreneTFSI / PEO blend. *Solid State Ionics*, pages 5–9, 2013.

[45] Ludvig Edman, Anders Ferry, and Greger Orädd. Analysis of diffusion in a solid polymer electrolyte in the context of a phase-separated system. *Physical Review E*, 65(4):042803, April 2002.

[46] Matthew D. Jensen. *Introduction to Computational Chemistry*. John Wiley & Sons Ltd, Chichester, 2nd edition, 2007.

[47] Florian Muller-Plathe. Local Structure and Dynamics in Solvent-Swollen Polymers. *Macromolecules*, 29:4782–4791, 1996.

[48] Jan-Michael Y Carrillo and Andrey V Dobrynin. Detailed molecular dynamics simulations of a model NaPSS in water. *The journal of physical chemistry. B*, 114(29):9391–9, July 2010.

[49] Grant D Smith, Chakravarthy Ayyagari, Richard L Jaffe, Matthew Pekny, and Aaron Bernarbo. Conformations of 2 , 4-Diphenylpentane : A Quantum Chemistry and Gas-Phase Molecular Dynamics Simulation Study. *J. Phys. Chem. A*, 102:4694–4702, 1998.

[50] E. A. Zubova, N. K. Balabaev, and L. I. Manevitch. Molecular mechanisms of the chain diffusion between crystalline and amorphous fractions in polyethylene. *Polymer*, 48:1802–1813, March 2007.

[51] Javier Pozuelo, Francisco Mendicuti, and Enrique Saiz. Conformations and mobility of polyethylene and trans -polyacetylene chains con ® ned in a -cyclodextrins channels q. *Polymer*, 43:523–531, 2002.

[52] Joseph Marie Thijssen. *Computational Physics*. Cambridge University Press, Cambridge, UK, 1999.

[53] D J Tildesley M. P. Allen. *Computer Simulation of Liquids*. Oxford University Press, Oxfrod, UK, 1989.

[54] W. Kohn P. Hohenberg. Inhomogeneous Electron Gas. *Physical Review*, 136:B 864 – B 871, 1964.

[55] Kieron Burke. Perspective on density functional theory. *The Journal of chemical physics*, 136(15):150901, April 2012.

[56] L. J. Sham W. Kohn. Self-Consistent Equations Including Exchange and Correlation Effects. *Physical Review*, 140:A 1133 – A 1138, 1965.

[57] W Smith, T R Forester, I T Todorov, and M Leslie. THE DL POLY 2 USER MANUAL, 2006.

[58] Axel D. Becke. Density-functional thermochemistry. III. The role of exact exchange. *The Journal of Chemical Physics*, 98(7):5648, 1993.

[59] M. J. Frisch, G. W. Trucks, H. B. Schlegel, G. E. Scuseria, M. A. Robb, J . R. Cheeseman, J. A. Montgomery Jr., T. Vreven, K. N. Kudin, J. C. Burant, J. M. Millam, S. S. Iyengar, J. Tomasi, V. Barone, B. Mennucci, M. Cossi, G. Scalmani, N. Rega, G. A. Petersson, H. Nakatsuji, M. Hada, M. Ehara, K. Toyota, R. Fukuda, J. Hasegawa, M. Ishida, T. Nakajima, Y. Honda, O. Kitao, H. Nakai, M. Klene, X. Li, J. E. Knox, H. P. Hratchian, J. B. Cross, V. Bakken, C. Adamo, J. Jaramillo, R. Gomperts, R. E. Stratmann, O. Yazyev, A. J. Austin, R. Cammi, C. Pomelli, J. W. Ochterski, P. Y. Ayala, K. Morokuma, G. A. Voth, P. Salvador, J. J. Dannenberg, V. G. Zakrzewski, S. Dapprich, A. D. Daniels, M. C. Strain, O. Farkas, D. K. Malick, A. D. Rabuck, K. Raghavachari, J. B. Foresman, J. V. Ortiz, Q. Cui, A. G. Baboul, S. Clifford, J. Cioslowski, B. B. Stefanov, G. Liu, A. Liashenko, P. Piskorz, I. Komaromi, R. L. Martin, D. J. Fox, T. Keith, M. A. Al-Laham, C. Y. Peng, A. Nanayakkara, M. Challacombe, P. M. W. Gill, B. Johnson, W. Chen, M. W. Wong, C. Gonzalez, and J. A. Pople. Gaussian 03. Revision C.02, Gaussian, Inc., Wallingford, CT, 2004.

[60] Endel Soolo, Jaanus Karo, Heiki Kasemägi, Maarja Kruusmaa, and Alvo Aabloo. Application of the Monte Carlo method for creation of initial models of EAP molecules for Molecular Dynamics simulation. In Yoseph Bar-Cohen, editor, *SPIE Vol. 6168*, volume 6168, pages 61682A–61682A–12, March 2006.

[61] W Smith and T R Forester. DL _ POLY _ 2 . 0 : A general-purpose parallel molecular dynamics simulation package Overall design. *Journal of Molecular Graphics*, 14:136–141, 1996.

[62] Ilian T. Todorov, William Smith, Kostya Trachenko, and Martin T. Dove. DL_POLY_3: new dimensions in molecular dynamics simulations via massive parallelism. *Journal of Materials Chemistry*, 16(20):1911, 2006.

[63] William G Hoover. Canonical dynamics: Equilibrium phase-space distributions. *Physical Review A*, 31:1695–1697, 1985.

[64] Simone Melchionna, Giovanni Ciccotti, and Brad Lee Holian. Hoover NPT dynamics for systems varying in shape and size. *Molecular Physics*, 78(3):533–544, 1993.

[65] Oleg Borodin and Grant D. Smith. Mechanism of Ion Transport in Amorphous Poly(ethylene oxide)/LiTFSI from Molecular Dynamics Simulations. *Macromolecules*, 39(4):1620–1629, February 2006.

Appendix A

Force field parameters

Atomtype	CPE-CPEC-CPO-OPO	CA0-CPEC-CPO-OPO
A_0	4.571	4.571
A_1	3.755	3.755
ϕ_1	84.8	-40.2
A_2	1.254	1.254
ϕ_2	-98.3	11.7
A_3	2.964	2.964
ϕ_3	17.2	2.2
A_4	0.526	0.526
ϕ_4	159.9	19.9
A_5	0.219	0.219
ϕ_5	-46.7	48.3
A_6	0.262	0.262
ϕ_6	82.52	
A_7	0.197	0.197
ϕ_7	162.7	

Table A.1: Dihedrals: CPE-CPEC-CPO-OPO and CA0-CPEC-CPO-OPO

Atomtype	HPEC-CPEC-CPO-OPO	CH-CPE-CPEC-CPE	CH-CPE-CPEC-CA0
A_0	4.571	5.712	5.712
A_1	3.755	4.545	4.545
ϕ_1	-157.7	60.69	-64.312
A_2	1.254	1.425	1.425
ϕ_2	136.7	-149.4	-39.44
A_3	2.964	2.72	2.72
ϕ_3	9.74	-21.13	-36.13
A_4	0.526	0.352	0.352
ϕ_4	-90.1	34.92	-105.1
A_5	0.219	0.0767	0.0767
ϕ_5	-179.2	-95.05	-0.048
A_6	0.262	0.238	0.238
ϕ_6	67.0	-26.87	-56.87
A_7	0.197	0.191	0.191
ϕ_7	-95.5	16.68	-138.3

Table A.2: Dihedrals: HPEC-CPEC-CPO-OPO, CH-CPE-CPEC-CPE ans CH-CPE-CPEC-CA0

Atomtype	CH-CPE-CPEC-HPE	HPO-CPO-CH-CPE
A_0	5.712	5.878
A_1	4.545	7.105
ϕ_1	178.2	151.1
A_2	1.425	4.146
ϕ_2	85.56	-55.82
A_3	2.72	2.32
ϕ_3	-28.63	55.04
A_4	0.352	0.232
ϕ_4	144.92	-97.7
A_5	0.0767	0.491
ϕ_5	132.45	-155.4
A_6	0.238	0.656
ϕ_6	-41.87	0.57
A_7	0.191	0.531
ϕ_7	119.2	151.98

Table A.3: Dihedrals: CH-CPE-CPEC-HPE and HPO-CPO-CH-CPE

Atomtype	OPO-CPO-CH-CPE	CPO-CH-CPE-CPEC	CPO-CH-CPE-HPE
A_0	5.878	7.753	7.753
A_1	7.105	10.04	10.04
ϕ_1	-15.9	-15.896	106.6
A_2	4.146	5.616	5.616
ϕ_2	-43.24	-43.24	-158.2
A_3	2.32	3.212	3.212
ϕ_3	-45.58	-45.58	-38.08
A_4	0.232	0.538	0.538
ϕ_4	-75.72	-75.72	54.28
A_5	0.491	0.265	0.265
ϕ_5	18.88	18.88	-88.62
A_6	0.656	0.405	0.405
ϕ_6	21.21	21.206	36.21
A_7	0.531	0.3246	0.3246
ϕ_7	6.254	6.254	143.75

Table A.4: Dihedrals: OPO-CPO-CH-CPE, CPO-CH-CPE-CPEC and CPO-CH-CPE-HPE

Lihtlitsents lõputöö reprodutseerimiseks ja lõputöö üldsusele kättesaadavaks tegemiseks

Mina, _____Madis Ollikainen_____,
(autori nimi)

1. annan Tartu Ülikoolile tasuta loa (lihtlitsentsi) enda loodud teose
_____Computer simulations of single-ion BAB triblock copolymer electrolyte material for lithium-polymer batteries_____,
(lõputöö pealkiri)

mille juhendaja on _____Heiki Kasemägi_____,
(juhendaja nimi)

1.1. reprodutseerimiseks säilitamise ja üldsusele kättesaadavaks tegemise eesmärgil, sealhulgas digitaalarhiivi DSpace-is lisamise eesmärgil kuni autoriõiguse kehtivuse tähtaja lõppemiseni;

1.2. üldsusele kättesaadavaks tegemiseks Tartu Ülikooli veebikeskkonna kaudu, sealhulgas digitaalarhiivi DSpace´i kaudu alates **01.06.2016** kuni autoriõiguse kehtivuse tähtaja lõppemiseni.

2. olen teadlik, et nimetatud õigused jäävad alles ka autorile.

3. kinnitan, et lihtlitsentsi andmisega ei rikuta teiste isikute intellektuaalomandi ega isikuandmete kaitse seadusest tulenevaid õigusi.

Tartus, **27.05.2014**